X-321-68-158
PREPRINT

NASA TM X- 63238

FINITE ELEMENT MODELLING OF THREE-DIMENSIONAL STRUCTURES

GPO PRICE $ _____

CFSTI PRICE(S) $ _____

Hard copy (HC) 3.00

Microfiche (MF) .65

ff 653 July 65

MAY 1968

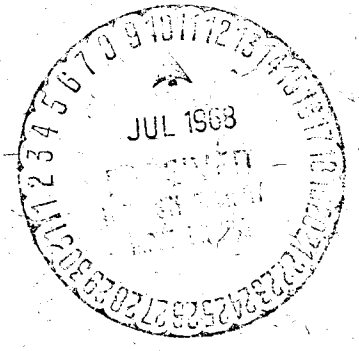

GSFC

GODDARD SPACE FLIGHT CENTER

GREENBELT, MARYLAND

X-321-68-158

FINITE ELEMENT MODELLING OF THREE-DIMENSIONAL STRUCTURES

Test and Evaluation Division
Systems Reliability Directorate

May 1968

GODDARD SPACE FLIGHT CENTER
Greenbelt, Maryland

FINITE ELEMENT MODELLING
OF THREE-DIMENSIONAL STRUCTURES

Prepared by: William R. Case Jr.
William R. Case, Jr.
Structural Analysis Computer Group

Reviewed by: Thomas G. Butler
Thomas G. Butler
Head, Structural Analysis Computer Group

Approved by: John H. Boeckel
John H. Boeckel
Deputy Chief, Test and Evaluation Division

PROJECT STATUS

This report describes the initial effort in obtaining a suitable three-dimensional finite element for use in the NASA NASTRAN program for structural analysis by the finite element technique.

AUTHORIZATION

Test and Evaluation Division charge number:

321-124-08-05-14

FINITE ELEMENT MODELLING OF THREE-DIMENSIONAL STRUCTURES

By

William R. Case, Jr.
Goddard Space Flight Center

SUMMARY

A three-dimensional finite element originally devised by A. Hrennikoff has been used to determine its accuracy in predicting the deflections, stresses and strains of an elastic continuum. This finite element model is of rectangular parallelepiped shape and is essentially a constant stress-strain element. In order to gauge its accuracy, a classic problem in three-dimensional elasticity with a known closed form solution was selected and this structure was modelled with the Hrennikoff finite element. The problem selected for this initial investigation was that of a prismatical bar stretching due to the action of its own weight. The results of the finite element analysis show excellent agreement with the theory even for a very coarse mesh size subdivision of the prismatical bar thereby indicating that the Hrennikoff finite element model can be used with confidence to model three-dimensionally elastic structures. Limitations on the application of this element are indicated in the text.

CONTENTS

TABLES

LIST OF ILLUSTRATIONS

LIST OF ILLUSTRATIONS (Continued)

FINITE ELEMENT MODELLING OF THREE-DIMENSIONAL STRUCTURES

William R. Case, Jr.
Goddard Space Flight Center

INTRODUCTION

Finite element modelling techniques for the determination of displacements and stresses in elastic bodies have received considerable attention in the literature throughout the last several years due to the development of acceptable numerical methods for computer solution of large order matrix equations. In particular, a great deal of effort has been concerned with the development of the stiffness characteristics of what may be termed one and two-dimensional elastic elements such as beams and plates while little has been done with three-dimensional elasticity problems. In recent years, however, the analyst has developed a need for obtaining solutions to complicated structures such as heat shields, rocket engines, solid propellant boosters, etc., which are truly three-dimensionally elastic in their load carrying capability.

It is the intent of this project to investigate ways of modelling three-dimensional structures in an effort to obtain a suitable finite element stiffness matrix which may be used in the NASA NASTRAN program for finite element analysis of structures. This report is concerned with the first method investigated and with the comparison of the results with theoretical solutions for one particular application.

The three-dimensional finite element model selected for this first investigation was originally developed by A. Hrennikoff (Reference 1) and was selected for several reasons. It is one of the simplest approaches to obtaining a stiffness matrix to represent a three-dimensional elastic continuum, and also the corresponding approach for two-dimensional elements (e.g. plate bending elements) has been shown to yield excellent results.

FINITE ELEMENT MODEL

The method developed by Hrennikoff for devising a finite element model of a three-dimensional elastic continuum consists of replacing this continuum by a framework of rods capable of carrying tension and compression and pin-joined at the corners as shown in Figure 1. By a judicious choice for the areas of these tension-compression members the framework can be made to deform according to Hooke's law when it is loaded at its corners with concentrated forces that are statically equivalent to the uniform stresses on the elastic solid.

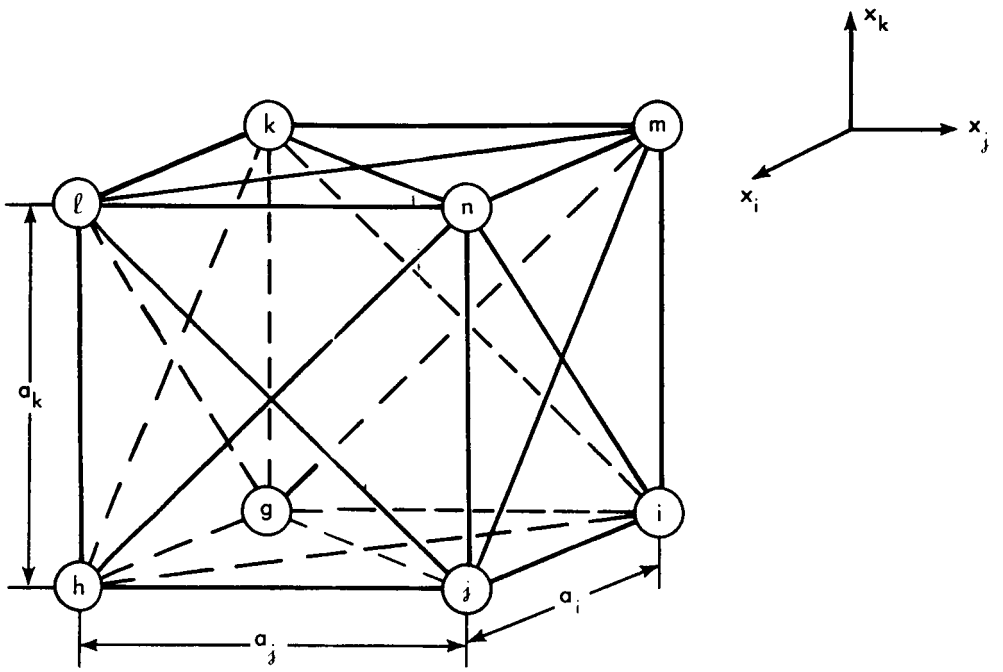

Figure 1. 3-D Hrennikoff Model

The actual calculation of the areas of the rods of the framework will not be carried out here since it is covered in detail for two-dimensional frameworks in References 1 and 2. In general, however, the procedure is as follows. We load the framework with concentrated loads at the grid points which are statically equivalent to the following uniform stress states:

1. Uniform normal stress σ in the x_i direction and $\nu\sigma$ in the x_j and x_k directions.

2. Uniform normal stress σ in the x_j direction and $\nu\sigma$ in the x_k and x_i directions.

3. Uniform normal stress σ in the x_k direction and $\nu\sigma$ in the x_i and x_j directions.

4. Uniform shear stress τ in each of the planes $x_i - x_j$, $x_j - x_k$ and $x_k - x_i$.

From these will result nine independent equations for elongations or shear of the framework in the various directions which are equated to those prescribed by

Hooke's law for an elastic volume under the action of the same stresses. Involved in these equations are nine parameters, namely the areas of the rods on the edges of the framework (A_i, A_j and A_k) parallel to the three axes; the areas of the rods that form the diagonals on the faces of the framework (A_{ij}, A_{jk} and A_{ki}); the ratios of two of the lengths of the framework to the other length and Poisson's ratio. It is found from these nine equations that the length ratios are arbitrary (i.e. we can make the framework the same size as the continuum we are modelling) and that Poisson's ratio (of the elastic continuum we are attempting to model) must have a value of: $\nu = 1/4$. The resulting rod areas are found to be:

$$A_i = \frac{a_0^2}{10} \rho_j \rho_k \beta_i$$

$$A_j = \frac{a_0^2}{10} \rho_k \rho_i \beta_j$$

$$A_k = \frac{a_0^2}{10} \rho_i \rho_j \beta_k \qquad (1)$$

$$A_{ij} = \frac{a_0^2}{10} \frac{\rho_k}{\rho_i \rho_j} (\rho_i^2 + \rho_j^2)^{3/2}$$

$$A_{jk} = \frac{a_0^2}{10} \frac{\rho_i}{\rho_j \rho_k} (\rho_j^2 + \rho_k^2)^{3/2}$$

$$A_{ki} = \frac{a_0^2}{10} \frac{\rho_j}{\rho_k \rho_i} (\rho_k^2 + \rho_i^2)^{3/2} \qquad (2)$$

Where

$$\beta_i = 4\left[1 - 1/4 \left(1 + \frac{\rho_i^2}{\rho_j^2} + \frac{\rho_i^2}{\rho_k^2}\right)\right]$$

$$\beta_j = 4\left[1 - 1/4 \left(1 + \frac{\rho_j^2}{\rho_k^2} + \frac{\rho_j^2}{\rho_i^2}\right)\right]$$

$$\beta_k = 4\left[1 - 1/4 \left(1 + \frac{\rho_k^2}{\rho_i^2} + \frac{\rho_k^2}{\rho_j^2}\right)\right] \qquad (3)$$

$$\rho_i = \frac{a_i}{a_0}, \quad \rho_j = \frac{a_j}{a_0}, \quad \rho_k = \frac{a_k}{a_0}$$

and a_0 is any reference length. The rather surprising result for the prescribed value of 1/4 for Poisson's ratio was originally discovered by Hrennikoff and is due to the fact that there are more stress conditions to satisfy than there are unknown rod areas. This difficulty can be avoided by adding more rods to the framework or by making the edge members beams that are rigidly connected to one another. For the purposes of this analysis, however, the value of $\nu = 1/4$ is acceptable and further complication of the model in order to free the restriction on Poisson's ratio is not warranted at this time.

If the rods of the framework have areas as given above, then the framework will deform exactly the same as the elastic solid if the solid is acted upon by uniform stresses and the framework is loaded at the grid points with statically equivalent concentrated forces. A three-dimensional elastic continuum can therefore be subdivided into small rectangular prisms and each of these in turn replaced by an equivalent framework whose rods have the areas prescribed above with the a_i, a_j, and a_k the size of the frameworks (i.e. the distances between grid points). This equivalent structure, consisting of all of the frameworks, is loaded at its grid points with concentrated forces that are obtained by lumping the actual body and surface forces acting on the elastic continuum. If the subdivision of the body is fine enough, the deflections of the finite element model will approach the true deflections of the elastic body.

Once the bar areas are known, the stiffness matrix of a single framework can be calculated by the standard methods. The development of the stiffness matrix is carried out in Appendix A for the 24 degrees of freedom (three translation degrees of freedom at each of the eight grid points of the framework). This stiffness matrix could be programmed into the NASTRAN program so that the user would have only to call for this element and from the grid point geometry and material property data input by the user the program would automatically calculate the stiffness matrices for all of the elements (frameworks) that comprise the structure. Since the general stiffness matrix, as shown in Table 1, has all of its coefficients in the form of simple algebraic equations, the calculation of this matrix by the program would require only a relatively short time.

Other three-dimensional finite elements may be more elaborate and for a given mesh size subdivision of a three-dimensional structure may give better results but would require more computer time to formulate the individual element stiffness matrices. Since the total computer time to solve a structures problem depends on the time to formulate the stiffness matrix for each element as well as the total number of grid points, it may be advantageous to use simple finite elements with a fine mesh subdivision of the structure as opposed to a coarser mesh with more elegant finite elements. At any rate, the simplicity of the Hrennikoff element, as depicted by its stiffness matrix in Table 1, is considered a definite advantage at this point.

As mentioned above, the Hrennikoff element stiffness matrix could be automated in the NASTRAN program although this has not been done and will not be done until other methods of modelling three-dimensional structures have been tried. In order to use the Hrennikoff element in the NASTRAN program at the present time the user must calculate the areas of all of the individual rods and input these to the program. The program does have rod elements and it will assemble all of the rods that make up the structure and solve the problem.

TEST PROBLEM

In general there are very few closed form solutions to three-dimensional elasticity problems that could be used as checkout problems for the three-dimensional finite element. Solutions that do exist fall into three major categories: closed form solutions to three-dimensional problems with finite boundaries, with boundaries at infinity, and approximate solutions to some classes of problems in the form of infinite series. Those in the first category are simple elasticity problems such as the bending of a three-dimensional beam, torsion of circular shafts and stretching of prismatical bars under the action of gravity loads. Within the second category lie such problems as the Boussinesq, Kelvin and Cerruti problems of forces acting on infinite or semi-infinite spaces. These latter problems can be used to check the finite element by making the model have specific finite dimensions and by applying conditions at the boundaries of the model that are the same as the exact elasticity solution prescribes at the corresponding points of the infinite medium. Such a method is discussed in Reference 3 in general and also specifically for the bending of a thick plate.

As a first trial for the 3-D Hrennikoff model, it was decided to use one of the simplier elasticity problems, in particular the stretching of a prismatical bar under the action of gravity loads. This problem is completely described in Reference 4 and only the solution will be presented here. For a bar as shown in Figure 2, under the action of its own weight and supported at the top such that the vertical deflection is zero at the point $x = y = 0$, $z = \ell$ and with a stress distribution of:

$$\sigma_x = \sigma_y = \tau_{xy} = \tau_{yz} = \tau_{zx} = 0$$

$$\sigma_z = \gamma z$$

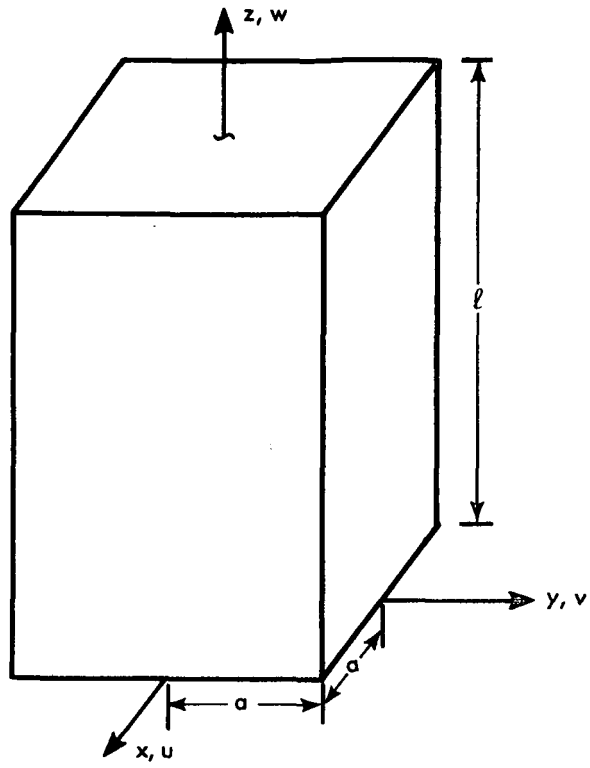

Figure 2. Prismatical Bar

The deflections of the bar are:

$$u = -\frac{\nu\gamma}{E} x z$$

$$v = -\frac{\nu\gamma}{E} y z$$

$$w = -\frac{\gamma}{2E}\left[(z^2 - \ell^2) + \nu(x^2 + y^2)\right]$$

where γ is the weight per unit volume of the bar.

For convenience we will nondimensionalize the deflections and stresses to the maximum vertical deflection along the z axis $\left(\frac{\gamma \ell^2}{2E}\right)$ and the maximum normal stress in the z direction $(\gamma\ell)$:

$$\bar{u} = \frac{2E}{\gamma \ell^2} u = -2\nu \left(\frac{a}{\ell}\right) \bar{x}\, \bar{z} \tag{5}$$

$$\bar{v} = \frac{2E}{\gamma \ell^2} v = -2\nu \left(\frac{a}{\ell}\right) \bar{y}\, \bar{z} \tag{6}$$

$$\bar{w} = \frac{2E}{\gamma \ell^2} w = (\bar{z}^2 - 1) + \nu \left(\frac{a}{\ell}\right)^2 (\bar{x}^2 + \bar{y}^2) \tag{7}$$

$$\bar{\sigma}_z = \frac{\sigma_z}{\gamma \ell} = \bar{z} \tag{8}$$

Where

$$\bar{x} = \frac{x}{a}, \quad \bar{y} = \frac{y}{a}, \quad \bar{z} = \frac{z}{a} \tag{9}$$

Equations (5) - (8) for the deflections and stresses are the exact solution to the bar hanging by its own weight and will be used as the basis of comparison for the finite element model results. The finite element model of the bar in Figure 2 is obtained by selecting a mesh size and replacing the elastic continuum within each mesh by the Hrennikoff frameworks as shown in Figure 3. Note that since the theoretical solution for w is symmetrical with respect to x and y and u and v are antisymmetrical, we can model only one quarter of the bar as indicated in Figure 3.

For the 1/4 model shown, a mesh size of 3 by 3 by 5 is indicated which means that the original continuum is now represented by 45 smaller volumes ($3 \times 3 \times 5$) each of which is a Hrennikoff framework of the type in Figure 1. The mesh size shown above was arbitrarily chosen and was used for several checkout problems in which the length of the bar was varied to determine whether the results would be more or less accurate for short stubby bars (in which Poisson's effect is large) than long slender ones. Other mesh sizes were chosen for a particular length bar to determine the rate of convergence of the finite element model results with mesh refinement. All computer runs were made on the IBM 7094/7040 DCS using the NASA NASTRAN program for finite element structural analysis by the displacement method (the force method will also be available at a later date). Solution times were all on the order of 10 minutes. The results of the finite element analyses together with the theoretical deflections and stresses for three different aspect ratio (a/ℓ) bars are shown in Figures 4-a through 6-c. All bars had a semi-width of $a = 3''$, and the three aspect ratios were obtained from bars of length 50", 10", and 6". In all three cases, the finite element mesh size was 3 by 3 by 5 as shown in Figure 3. The gravity loading,

$$Z = \gamma$$

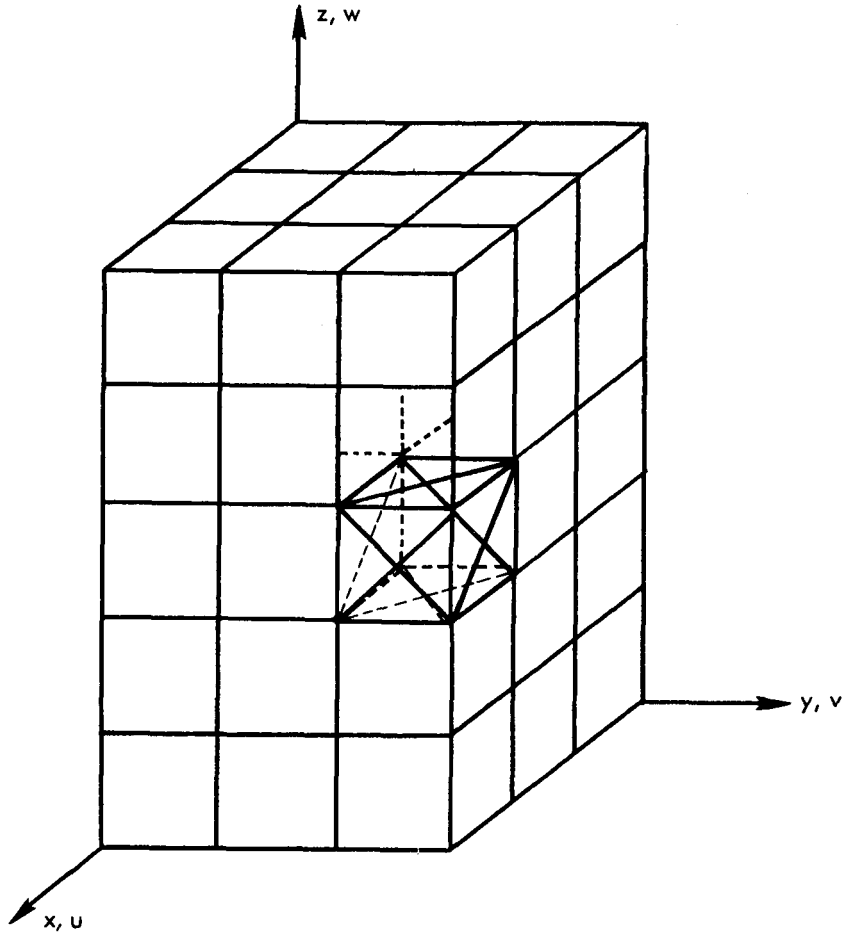

Figure 3. Finite Element Model of One Quarter of the Prismatical Bar (Mesh Size 3×3×5)

acting on the continuum was simulated on the finite element model by integrating over a volume around each grid point in the mesh and lumping the resultant load at the grid point. For each volume in the mesh, the equivalent Hrennikoff framework was made up from pin-jointed rods with areas given by Equation (2), taking i, j, and k to be the x, y, and z directions, respectively. Note that these equations give the areas of exterior rods, that is, those between two grid points not shared by another volume in the mesh. For two grid points that share rods from more than one framework, only one rod is used between these grid points that has the total area of all rods from the frameworks that connect between these grid points. Thus, along the × direction, for example, two grid points that are interior to the solid we are modelling will have four frameworks that

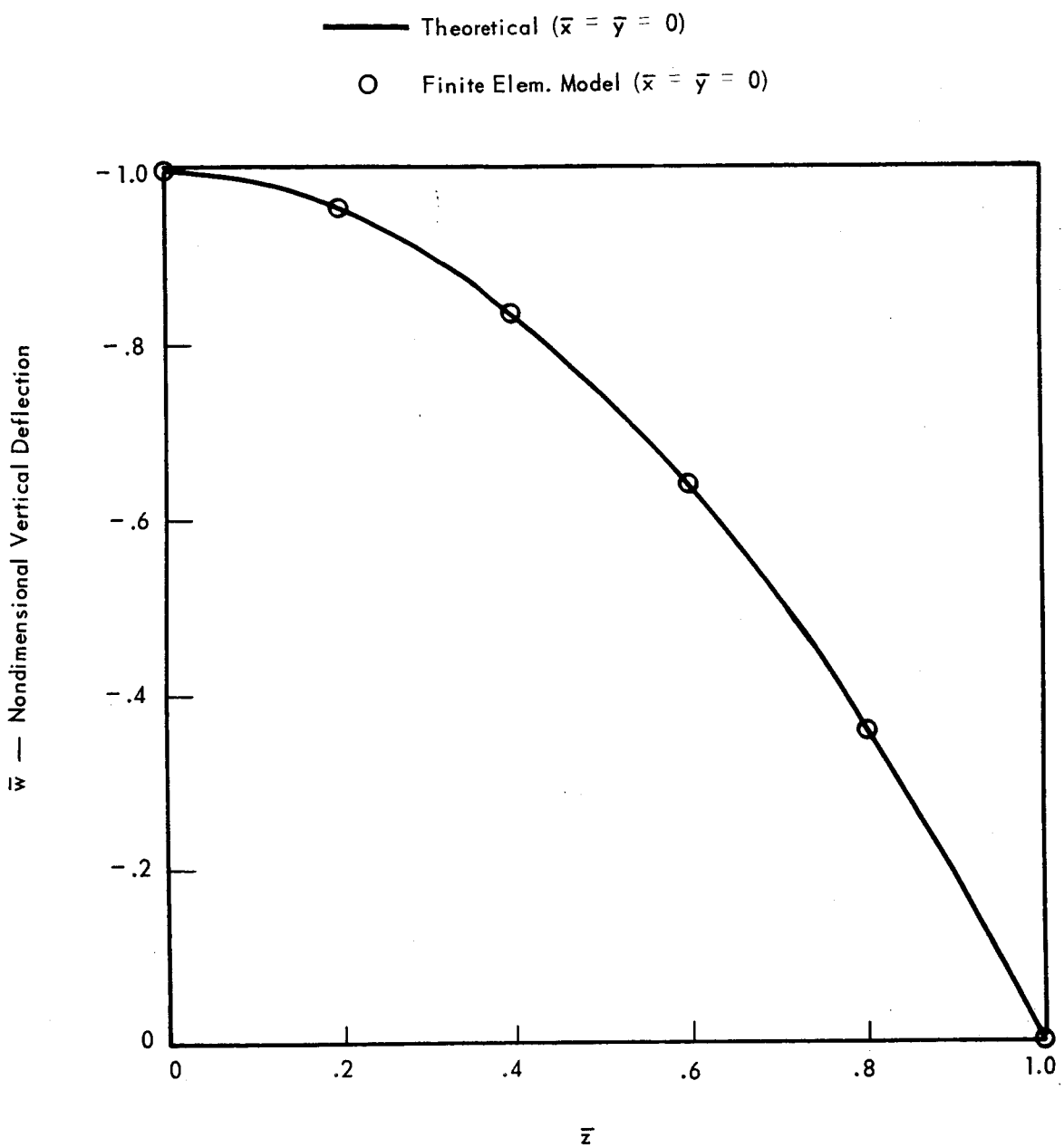

Figure 4a. Vertical Deflections for $a/\ell = .06$ (Finite Element Mesh Size $3 \times 3 \times 5$)

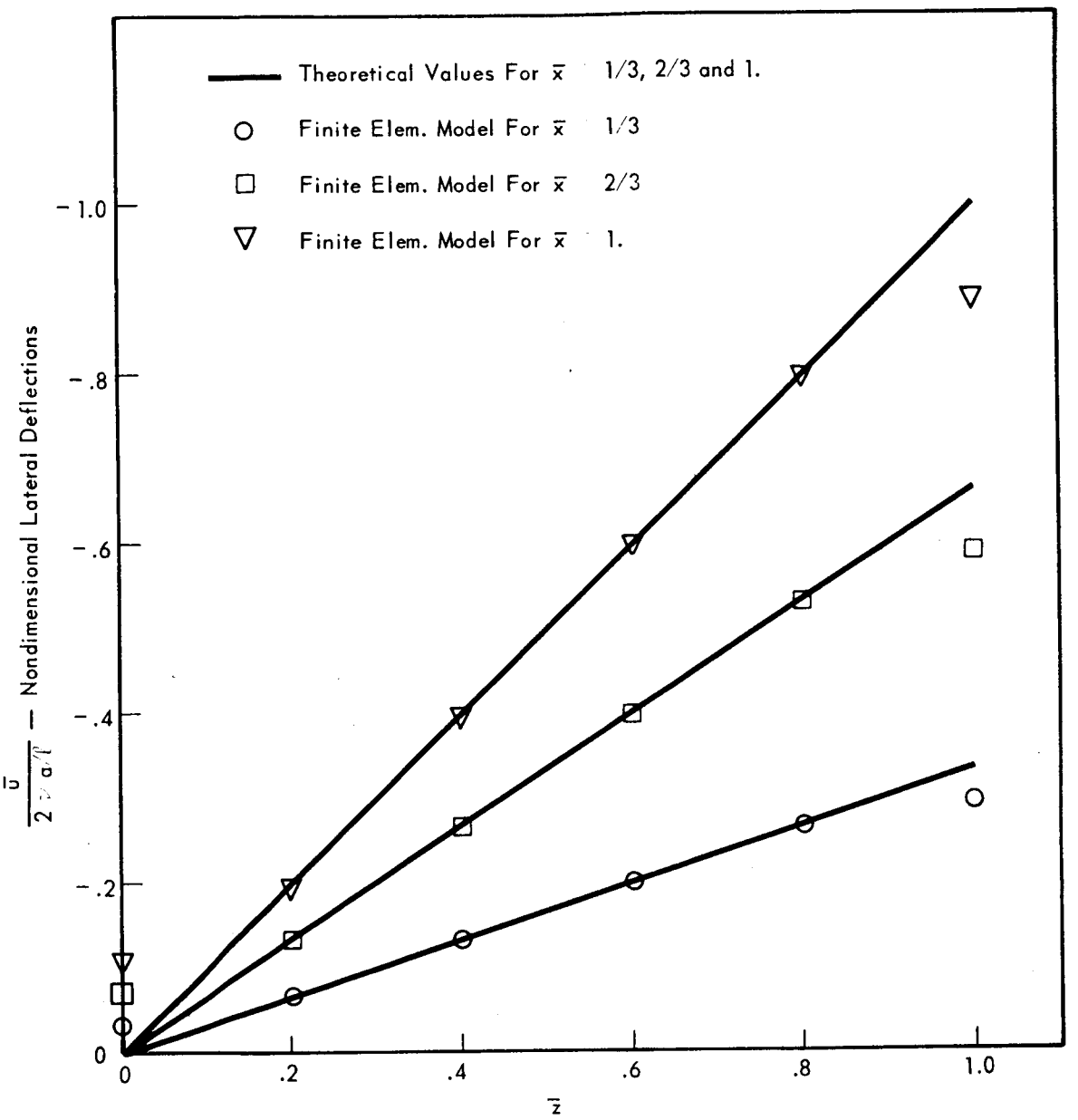

Figure 4b. Lateral Deflections for a/ℓ = .06 (Finite Element Model Mesh Size 3×3×5)

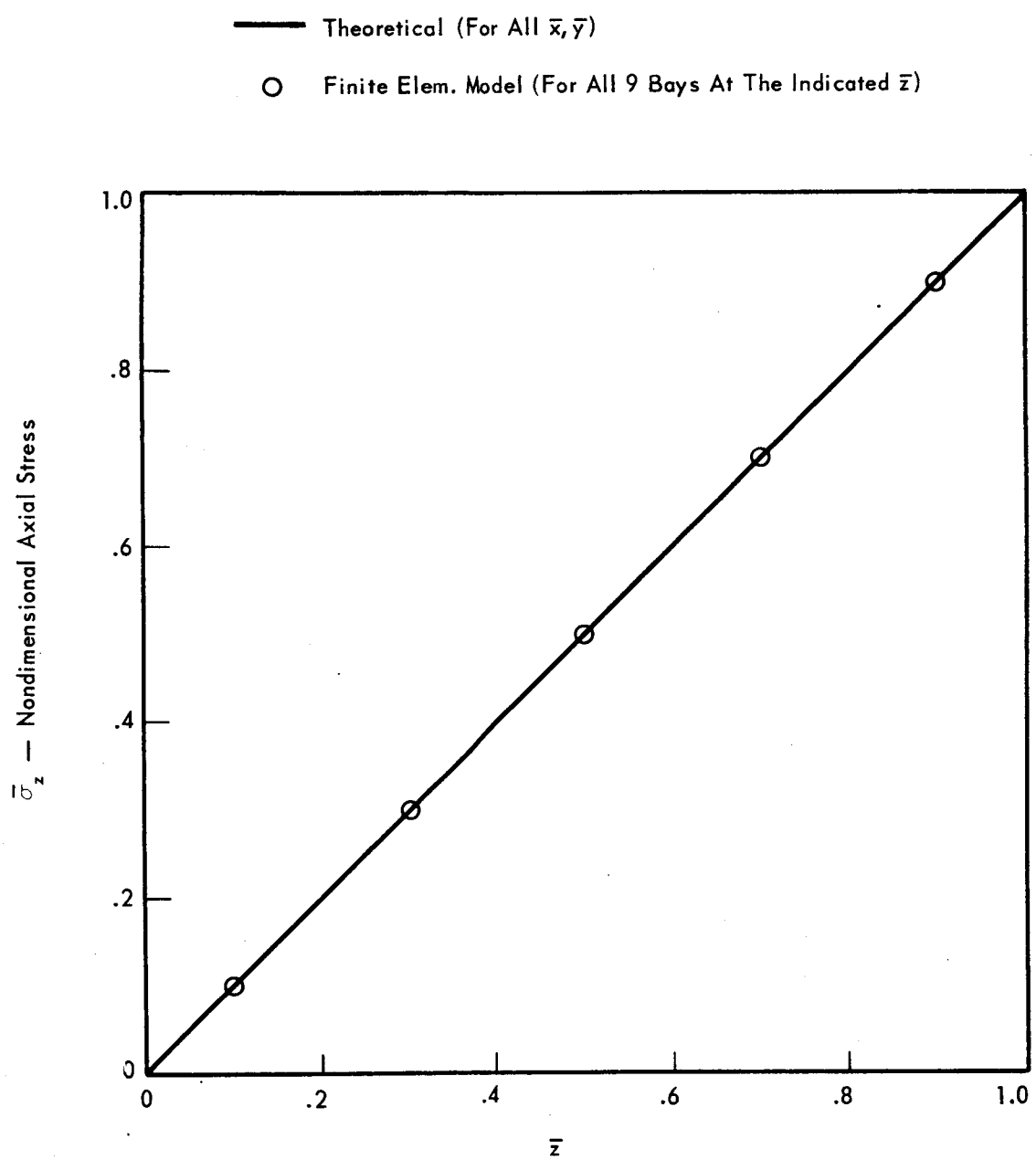

Figure 4c. Axial Stress for a/ℓ = .06 (Finite Element Mesh Size 3×3×5)

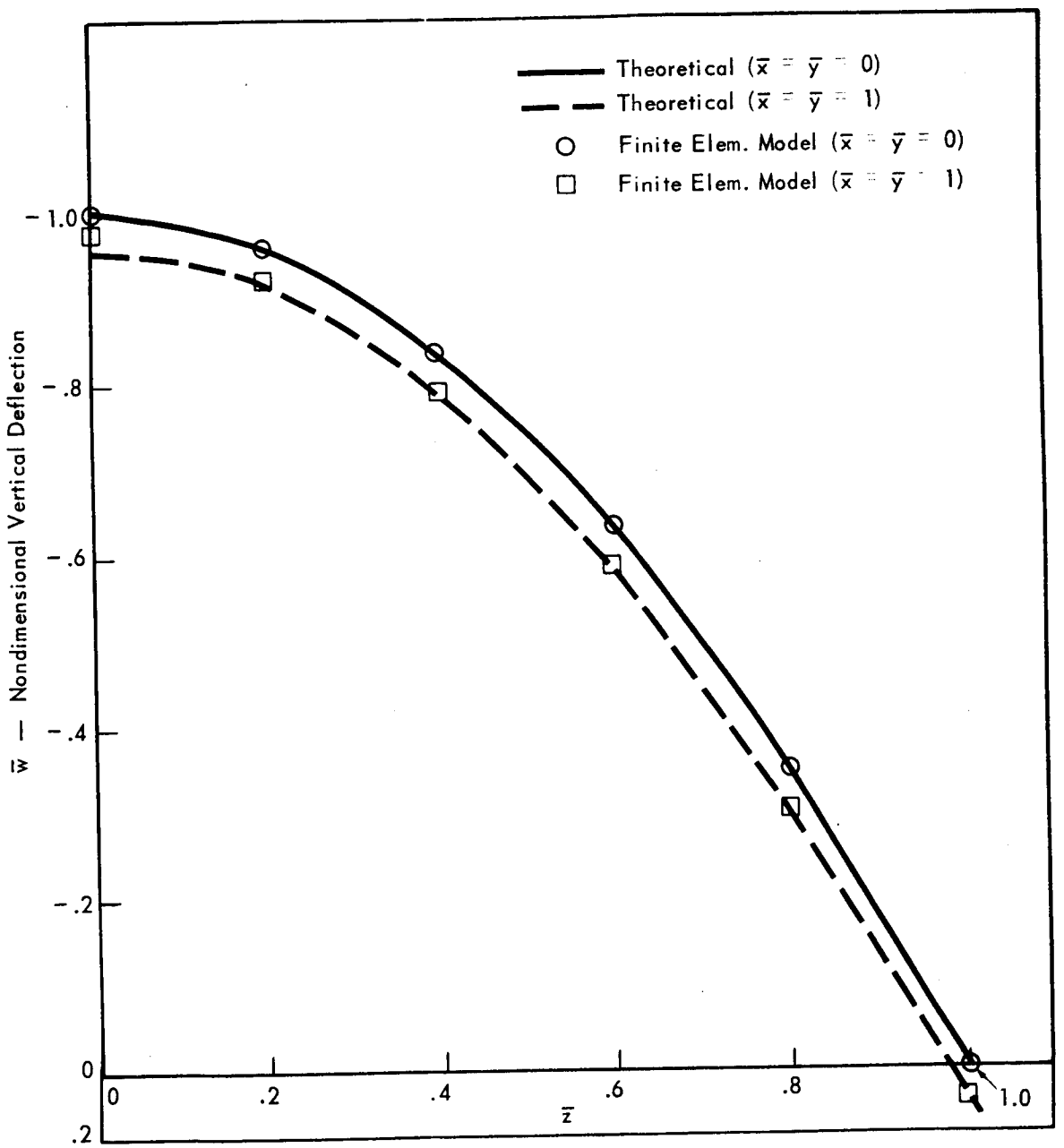

Figure 5a. Vertical Deflections for $a/\ell = .3$ (Finite Element Mesh Size $3 \times 3 \times 5$)

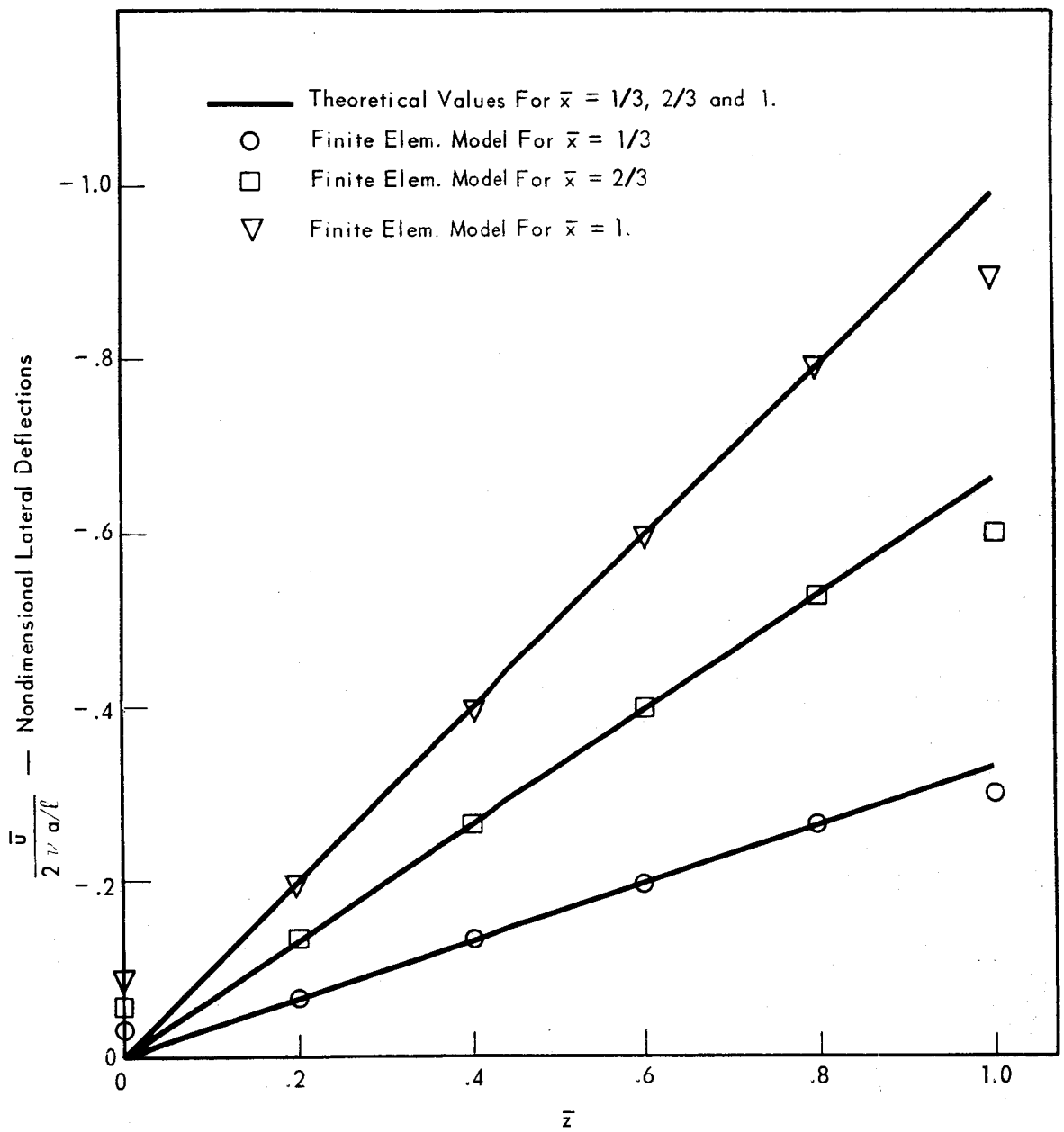

Figure 5b. Lateral Deflections for a/ℓ = .3 (Finite Element Mesh Size 3×3×5)

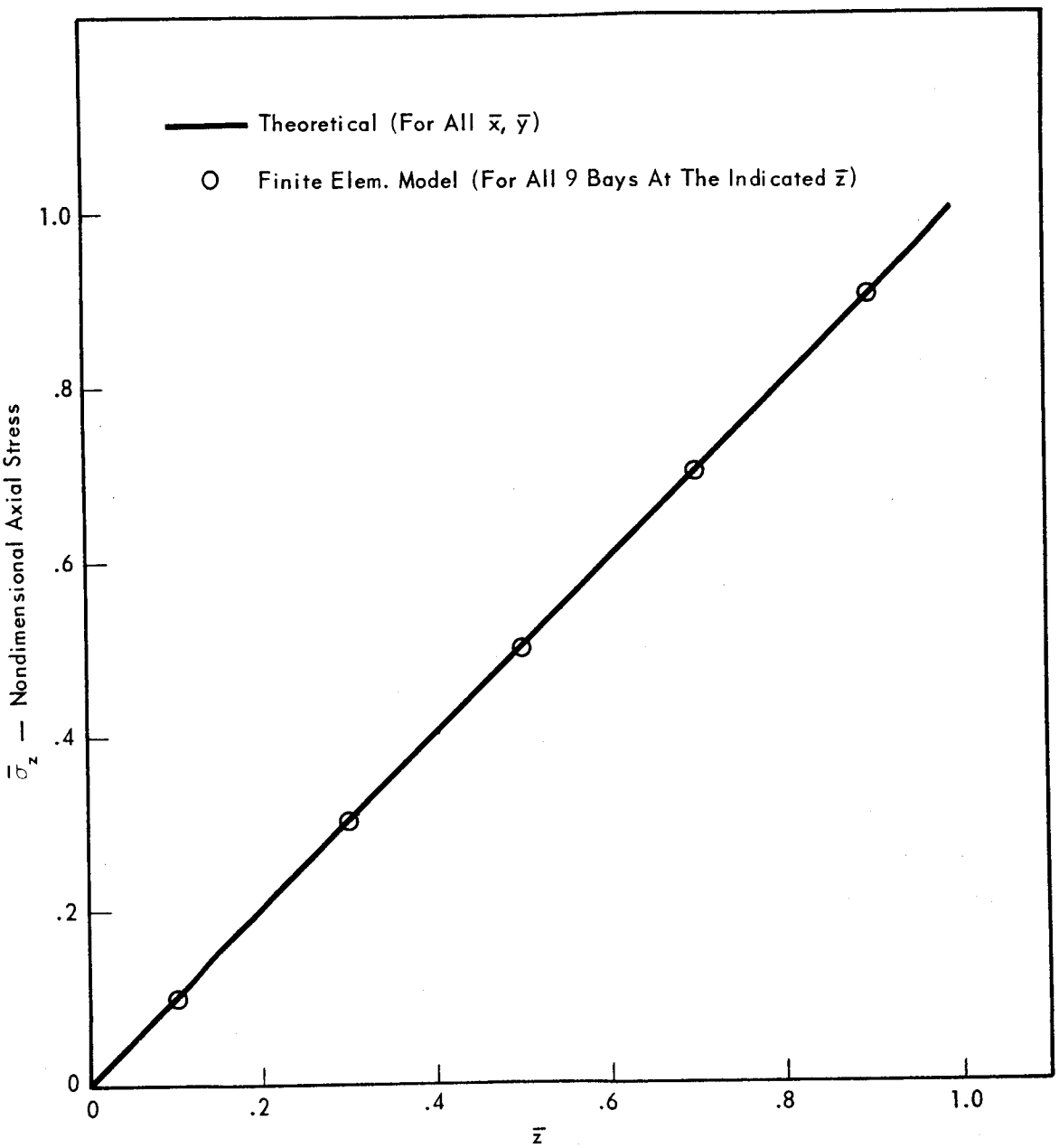

Figure 5c. Axial Stress for $a/\ell = .3$ (Finite Element Mesh Size $3 \times 3 \times 5$)

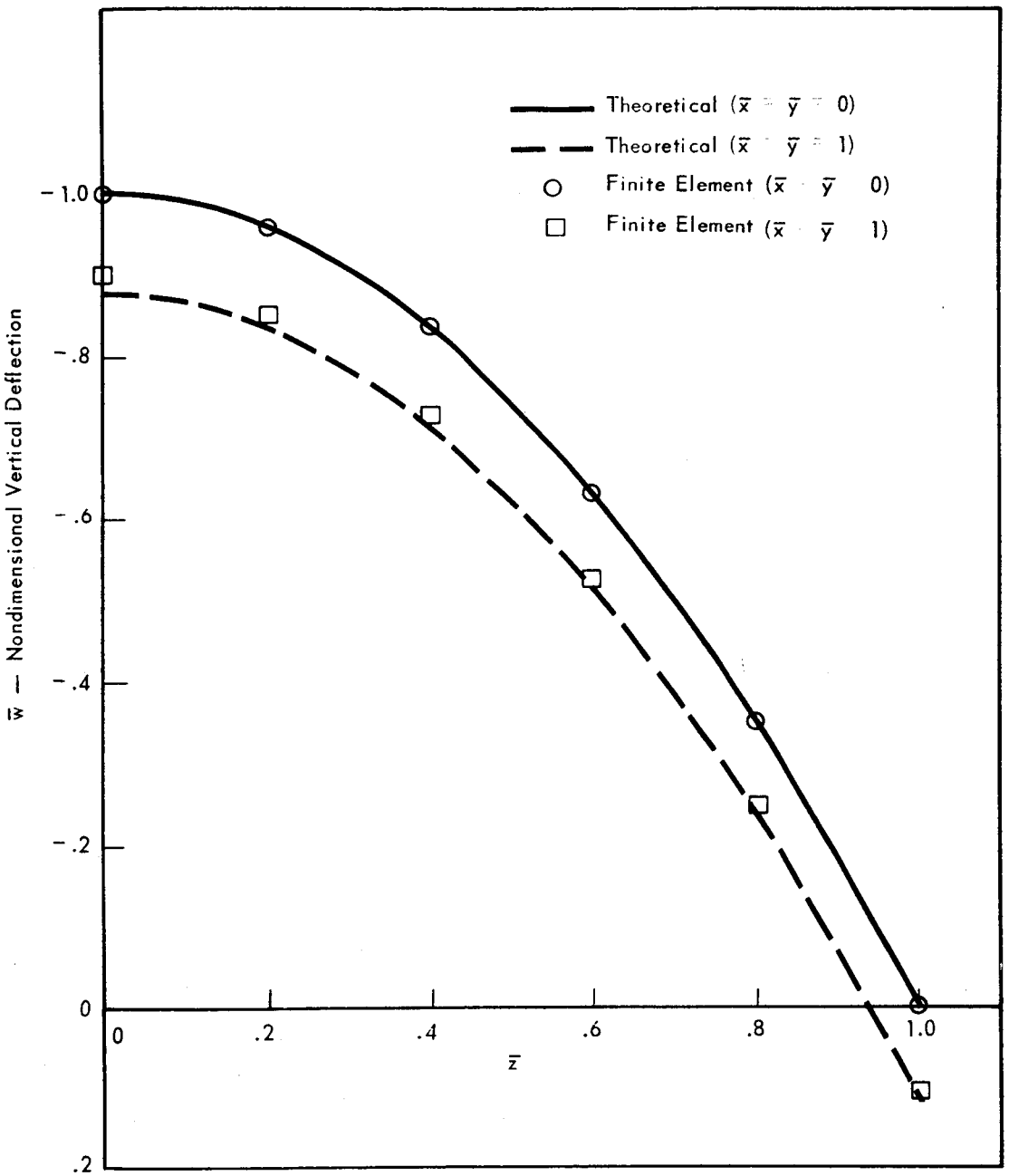

Figure 6a. Vertical Deflections for a/ℓ = .5 (Finite Element Mesh Size 3×3×5)

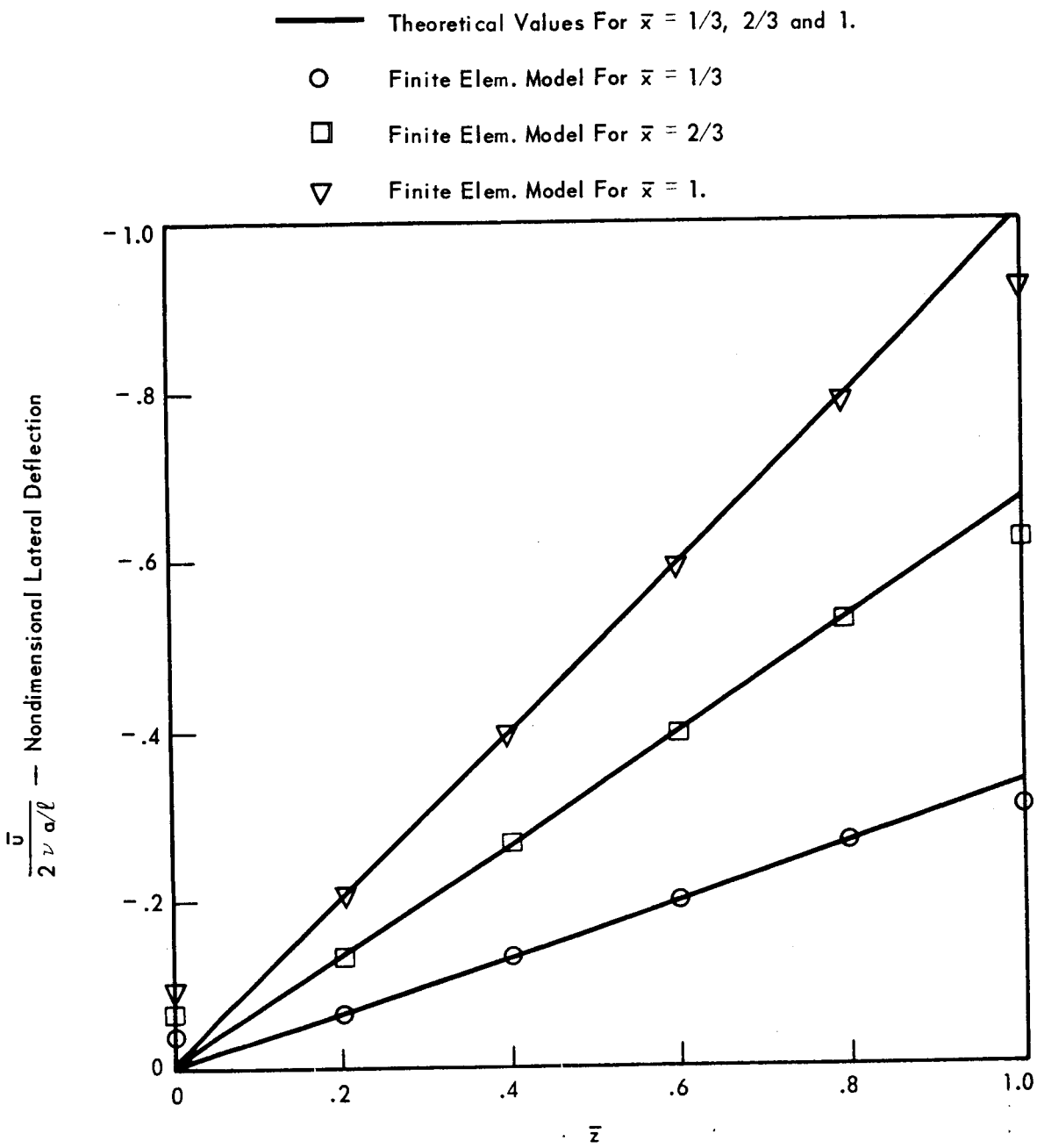

Figure 6b. Lateral Deflections for a/ℓ = .5 (Finite Element Mesh Size 3×3×5)

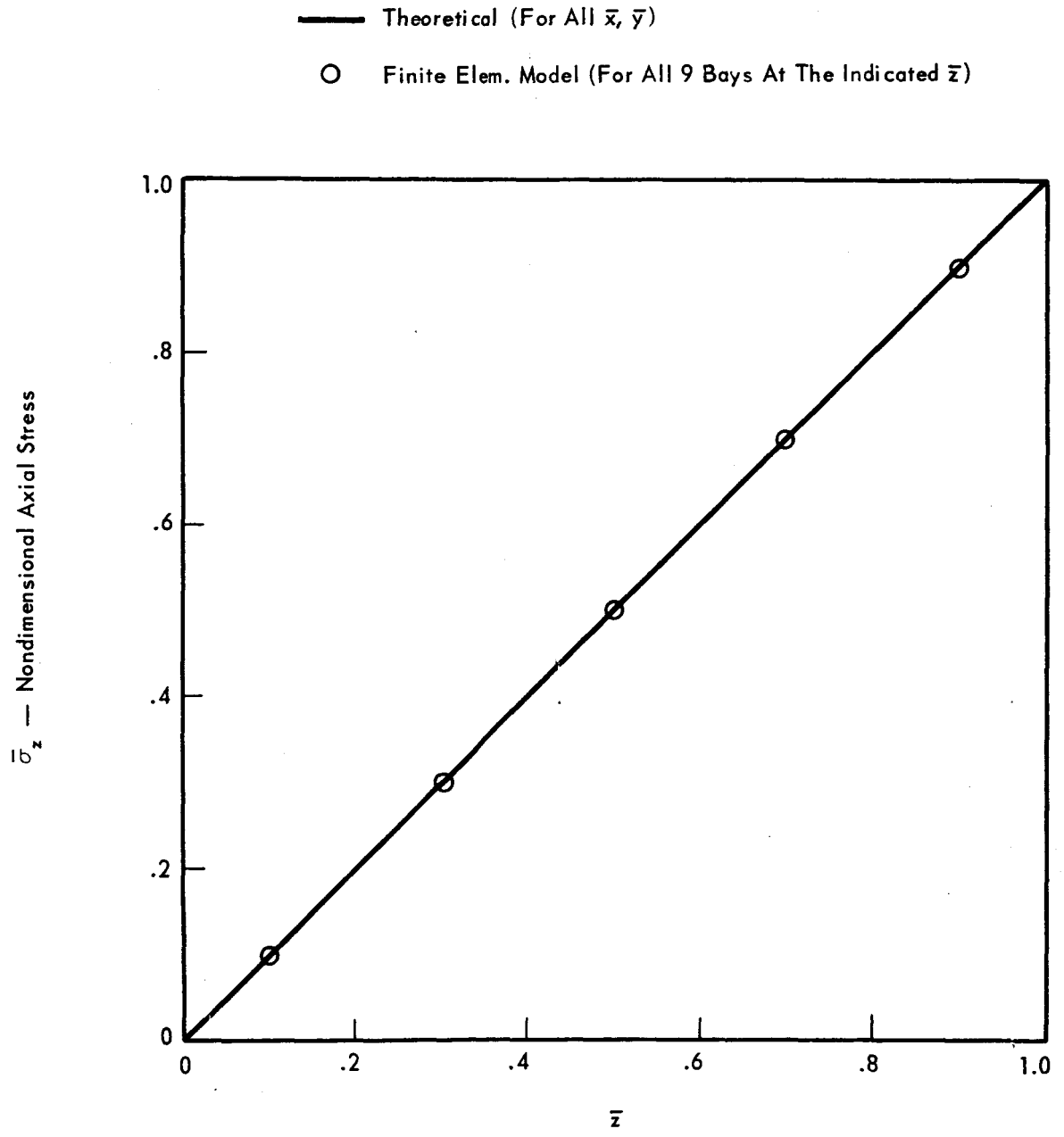

Figure 6c. Axial Stress for $a/\ell = .5$ (Finite Element Mesh Size $3 \times 3 \times 5$)

come together along a common edge thereby requiring that A_i, as given in Equation (2), be increased by a factor of four to obtain the single rod area between these two grid points.

As indicated in Figures 4-a, 5-a, and 6-a, the finite element results are in excellent agreement with the theory for the vertical deflections. Shown in these figures are the $\bar{w}$ deflections along the z axis as well as those along the furthest edge; $\bar{x} = \bar{y} = 1$ (except for the $a/\ell = .06$ case where the difference in the two is too small to show up). The $\bar{w}$ deflections along the $\bar{x} = \bar{y} = 1$ edge are where the maximum errors in any vertical deflection occur. Figures 4-b, 5-b, and 6-b show the nondimensionalized lateral deflection in the $\bar{x}$ direction and again the agreement is excellent except on the boundaries at $\bar{z} = 0$ and 1.0 where the error increases linearly with $\bar{x}$. Curves for the nondimensionalized lateral deflection in the $\bar{y}$ direction are not shown although they are exactly the same as those for the $\bar{x}$ direction if $\bar{x}$ is replaced by $\bar{y}$ in Figures 4-b, 5-b, and 6-b. That is, the finite element results yielded perfectly the symmetry condition:

$$u(x, y, z) = v(y, x, z)$$

which is due to the fact that $\partial\bar{u}/\partial\bar{x}$ and $\partial\bar{v}/\partial\bar{y}$ are identical as indicated by Equations (5) and (6).

The results for the stresses in the bar are shown on Figures 4-c, 5-c, and 6-c but were not obtained directly from the finite element computer runs. These were obtained by first calculating average strains using the grid point deflections and then converting these to stresses using Hooke's law. As such, they represent average stresses of the continuum over the volume bounded by the eight corner grid points of each framework. The figures show that the nondimensionalized axial stress, $\bar{\sigma}_z$ is in excellent agreement with the theory. All of the other stresses should be zero as indicated by Equation (4) and the results obtained for these from the grid point deflections indicated that the maximum stress other than $\bar{\sigma}_z$ was always less than 2% of the maximum $\bar{\sigma}_z$ which is unity.

For the bar with aspect ratio $a/\ell = .5$, several finite element analyses were performed for various mesh sizes to investigate the rate of convergence of the results with model mesh refinement. Besides the $3\times3\times5$ mesh discussed above, four other mesh sizes were employed, namely $1\times1\times2$, $2\times2\times4$, $3\times3\times6$, and $4\times4\times8$. Therefore, if M is designated as the mesh size (the total number of bays that the bar is subdivided into) and N is designated as the number of subdivisions along the x or y axis, then for these four problems:

$$M = (N)\ (N)\ (2N) = 2N^3$$

where N = 1, 2, 3, and 4. For the case N = 4 (i.e., the 4 × 4 × 8 mesh) the results for the vertical and lateral deflections and the axial stresses are shown in Figures 7-a, 7-b, and 7-c. As before for the $3\times3\times5$ mesh run of the bar with $a/\ell = .5$, the finite element results are in excellent agreement with the theory with the boundary errors decreasing over those for the $3\times3\times5$ mesh as would be expected. The solution time on the computer for the $4\times4\times8$ mesh model was approximately 16 minutes as compared to 8 minutes for the $3\times3\times5$ mesh.

Figure 8 shows the comparison of several of the finite element results for the $a/\ell = .5$ bar for the four mesh sizes selected (N = 1, 2, 3, and 4 in Equation (10)). The vertical deflection at the origin, the results of which are designated by the circled data points on Figure 8, are exact for all mesh sizes. This is due to the assumptions that went into the Hrennikoff model and the linearly varying stress state in the three-dimensional solid that is being modelled.

The vertical deflection at the corner $\bar{x} = \bar{y} = 1$ and $\bar{z} = 0$ is also shown since the largest magnitude error in any vertical deflection occurs here. As indicated by the curve, the finite element result converges to within approximately 1% of the theoretical value for the finest mesh size analyzed. Similarly, the boundary deflection in the lateral direction at $\bar{x} = \bar{z} = 1$ (for all $\bar{y}$) converges rapidly to the theoretical value also. The strain energy curve shown on the figure was obtained from the grid point deflections and the input grid point forces and is included since it gives a sort of weighted or average error of the deflections when compared to the theoretical strain energy. Even for the very coarse mesh size of $1\times1\times2$, all of the results shown on Figure 8 are much better than one would have anticipated. This is probably due to the nature of the problem investigated. Since the load is a distributed one which varies uniformly over the bar, one would expect to get better results for the same mesh size for this type problem than for one in which a single concentrated load or a nonuniform distributed load was acting.

CONCLUSIONS

On the basis of this single investigation, it is concluded that the Hrennikoff model may be used as a practical model for three-dimensional elasticity problems in which the stress distributions and boundary conditions do not vary rapidly over the boay. It has been shown that for a bar hanging by its own weight, this technique for modelling three-dimensional structures gives excellent results even for very coarse mesh sizes. Since the Hrennikoff model is a constant stress strain finite element, finer mesh sizes will have to be employed for three-dimensional elasticity problems in which the stress gradients are larger than those investigated here. This disadvantage may well be offset by the distinct

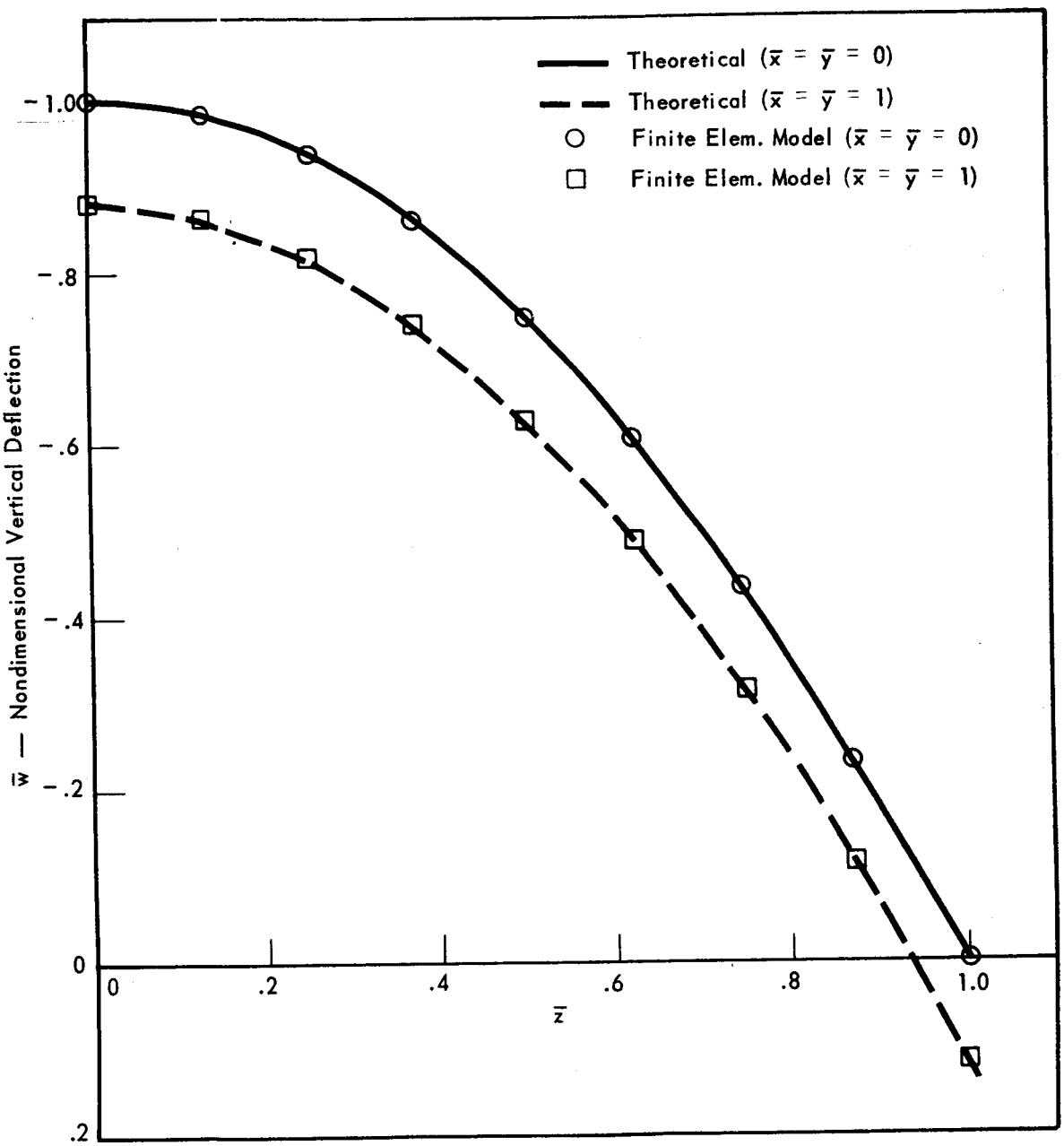

Figure 7a. Vertical Deflections for $a/\ell = .5$ (Finite Element Mesh Size $4 \times 4 \times 8$)

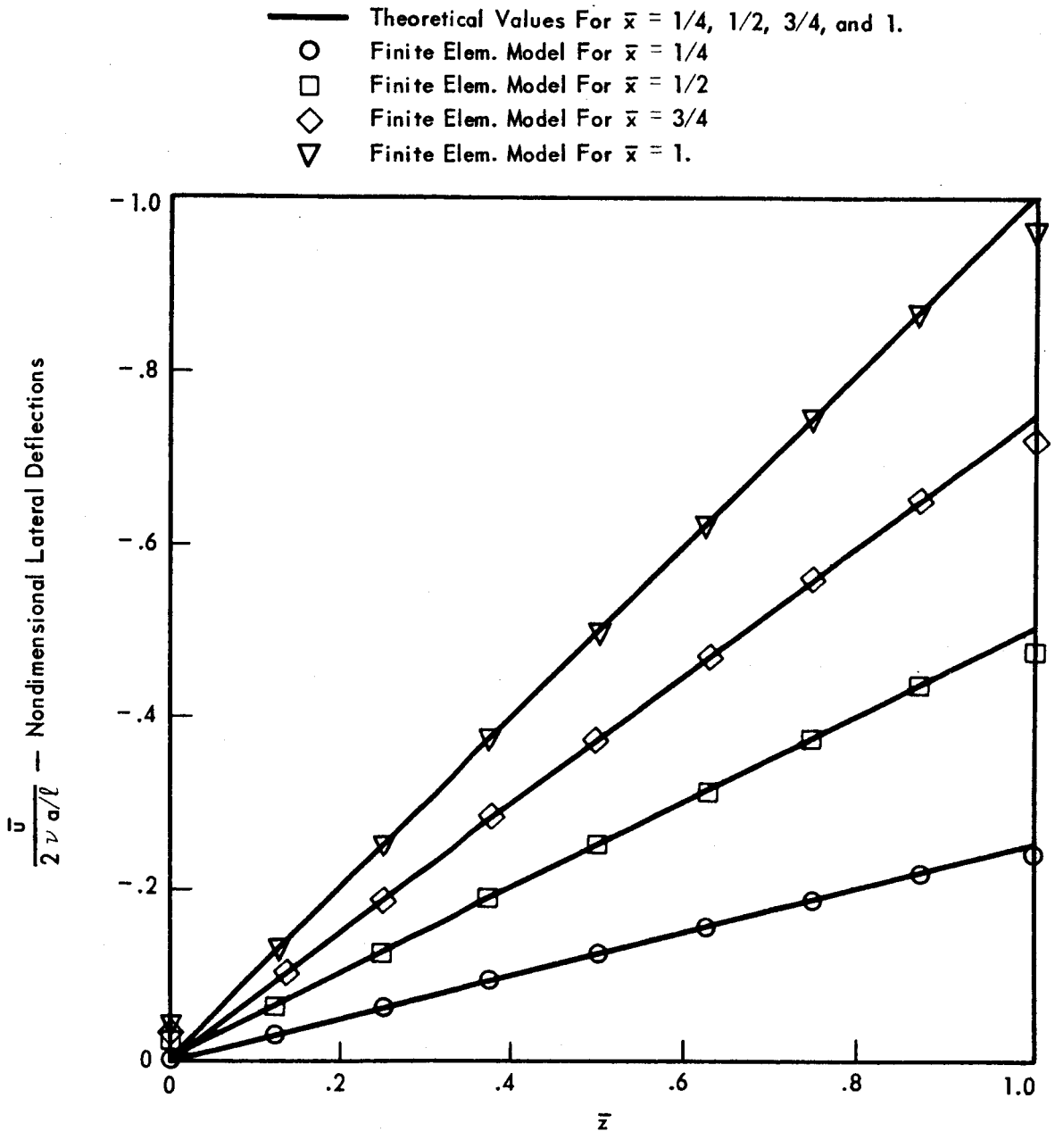

Figure 7b. Lateral Deflections for a/ℓ = .5 (Finite Element Mesh Size 4×4×8)

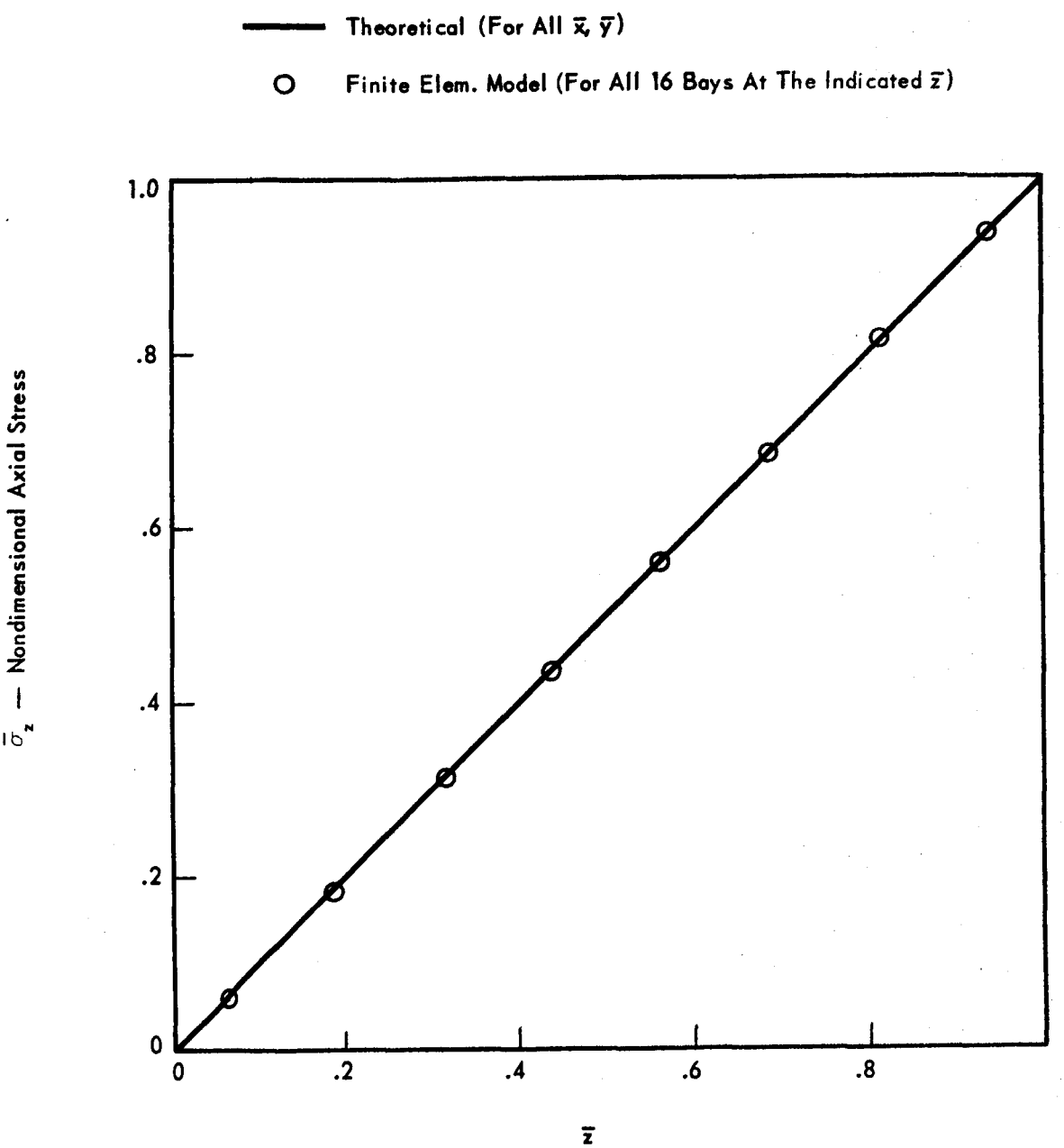

Figure 7c. Axial Stress for $a/\ell = .5$ (Finite Element Mesh Size $4 \times 4 \times 8$)

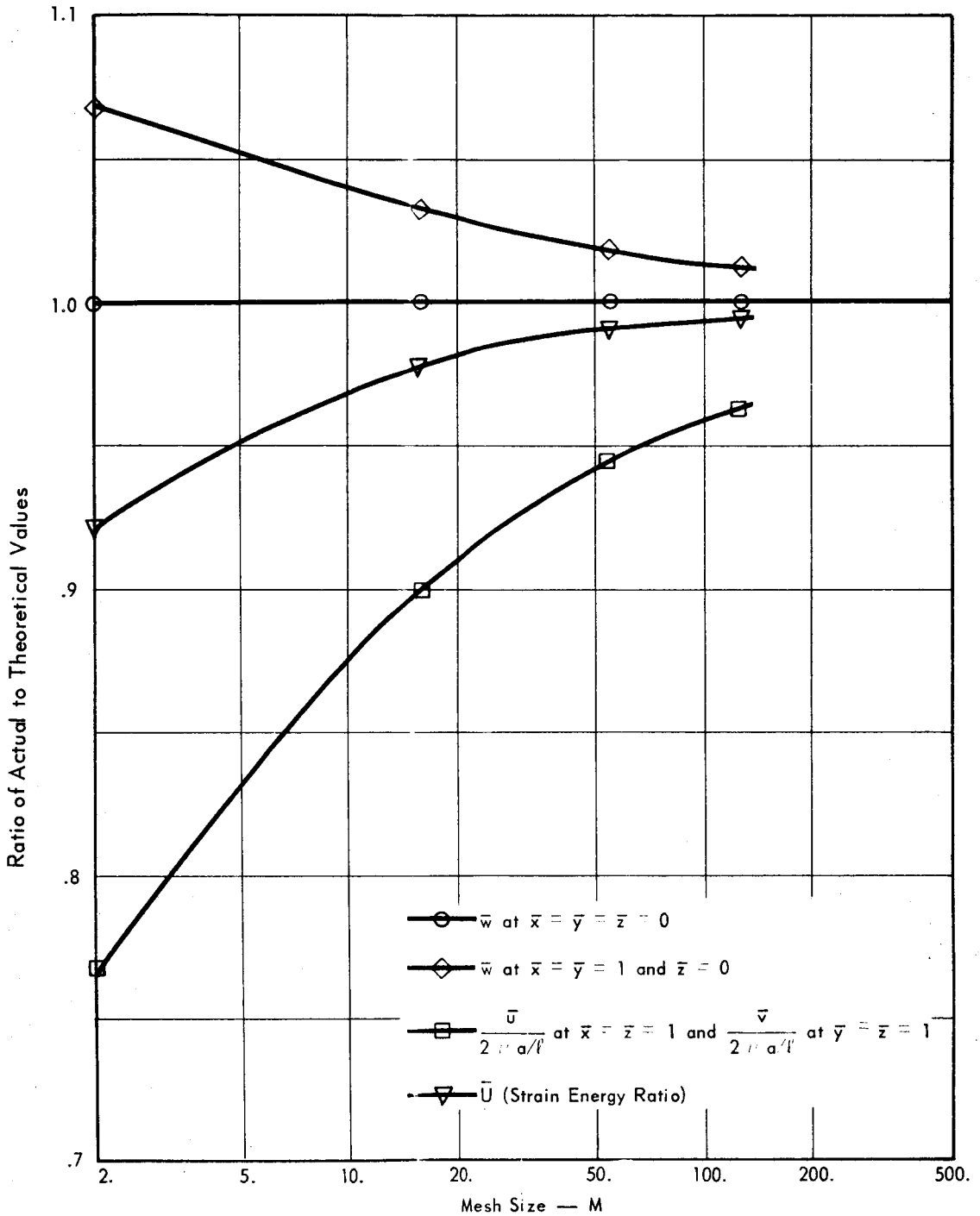

Note: Data points are for models with N bays in the x and y directions and 2N bays in the z direction (N 1, 2, 3 and 4) so that M $2N^3$.

Figure 8. Comparison of Results for Various Mesh Sizes for Bar with $a/\ell = 0.5$

advantage of the simplicity of the Hrennikoff model. As indicated on Table 1, the stiffness matrix for any aspect ratio Hrennikoff model is available in a closed form solution involving only algebraic expressions. As more complexity is built into other three-dimensional finite elements, their corresponding stiffness matrices will be more complex and thereby require more computer time to formulate. Although the more complex finite element will allow problems to be solved with coarser mesh sizes, this savings in computer time may be offset by the increase in computer time required to formulate the stiffness matrix.

Future work in this area of three-dimensional finite elements will be to investigate other methods of modelling three-dimensional bodies, to revise the Hrennikoff model to free the restriction on Poisson's ratio ($\nu = 1/4$), and to develop Hrennikoff shapes other than the rectangular parallelepiped.

REFERENCES

1. Hrennikoff, A. — Solution of Problems of Elasticity by the Framework Method, J. Appl. Mech., December 1941

2. Pestel, E. — Investigation of Plate and Shell Models by Matrices AFOSR Report No. 64-0592, May 1963

3. Greenspon, J. E. — Development of Analysis Procedures for Spacecraft Structures Under Dynamic Loading, Second Quarterly Report NASA Contract NAS 5-10262, December 1966

4. Timoshenko, S. and Goodier, J. N. — Theory of Elasticity, McGraw-Hill, Second Edition, 1951

APPENDIX A

3-D Hrennikoff Element Stiffness Matrix

The stiffness matrix for the Hrennikoff element is derived in a straightforward manner by considering the stiffness of each of the individual rods that make up the element and then assembling these into the overall stiffness matrix for the element. For the Hrennikoff element as shown in Figure 1 (Page 2) there are at most six different rods since all of those orientated parallel to any one axis are the same and all of those parallel to any plane are the same as indicated by the area equations in Section 2.

Using the notation of Equations (2) the stiffness matrix for any rod in the Hrennikoff element written in a local coordinate system with axis along this rod can be written as:

$$k_p = \frac{A_p E}{a_p} \begin{bmatrix} 1 & -1 \\ -1 & 1 \end{bmatrix} \qquad \text{A-(1)}$$

where p takes on the values i, j, and k to give the stiffness matrices for those rods parallel to either the x_i, x_j, or x_k axes (see Figure 1) and

$$k_{mn} = \frac{A_{mn} E}{a_{mn}} \begin{bmatrix} 1 & -1 \\ -1 & 1 \end{bmatrix} \qquad \text{A-(2)}$$

where mn take on the values ij, jk, and ki to give the stiffness matrices for the rods parallel to the $x_i - x_j$, $x_j - x_k$, and $x_k - x_i$ planes. The unassembled stiffness matrix for the Hrennikoff element is a matrix with the rod stiffness matrices on its diagonal and zero's elsewhere, denoting this as $\bar{K}$ we have:

$$\bar{K} = \begin{bmatrix} \bar{K}_i & & & & & \\ & \bar{K}_j & & & & \\ & & \bar{K}_k & & & \\ & & & \bar{K}_{ij} & & \\ & & & & \bar{K}_{jk} & \\ & & & & & \bar{K}_{ki} \end{bmatrix} \qquad \text{A-(3)}$$

where

$$\bar{K}_i = \begin{bmatrix} k_i & & & \\ & k_i & & \\ & & k_i & \\ & & & k_i \end{bmatrix} \qquad \text{A-(4)}$$

and k_i is given by Equation A-(1). Similar definitions hold for $\bar{K}_j$ and $\bar{K}_k$. For $\bar{K}_{ij}$, $\bar{K}_{jk}$, and $\bar{K}_{ki}$ these submatrices are defined similar to A-(4) but with A-(2) giving the form of the four diagonal matrices.

Equation A-(3) contains the stiffness matrices of all 24 rod elements (four each of six types) in coordinate systems oriented along each rod. In order to get the stiffness matrix for the Hrennikoff element in the x_i, x_j, and x_k coordinates we need to perform a coordinate transformation and apply joint (grid point) compatibility conditions, that is, we need to relate the individual rod degrees of freedom inherent in Equations A-(1) and A-(2) in local coordinates to the grid point degrees of freedom in the basis coordinates x_i, x_j, and x_k. This is accomplished by a pre and post multiplication of $\bar{K}$ in Equation A-(3) by a transformation matrix to give:

$$K = C^T \bar{K} C \qquad \text{A-(5)}$$

where K is the Hrennikoff element stiffness matrix (24 × 24) in terms of displacements in the x_i, x_j, and x_k coordinates of Figure 1 and C is a transformation matrix whose form is:

$$C = \begin{bmatrix} C_i & 0 & 0 \\ 0 & C_j & 0 \\ 0 & 0 & C_k \\ C_{ij} & \bar{C}_{ij} & 0 \\ 0 & C_{jk} & \bar{C}_{jk} \\ \bar{C}_{ki} & 0 & C_{ki} \end{bmatrix} \qquad \text{A-(6)}$$

The submatrices C_i, C_j etc. are 8 × 8 matrices that relate the degrees of freedom inherent in $\bar{K}_i$, $\bar{K}_j$ etc. to the grid point degrees of freedom of the Hrennikoff element. These submatrices in Equation A-(6) will not be presented here but are

easily found by geometrical considerations dependent on the ordering of the rod degrees of freedom and the Hrennikoff element corner point (grid point) degrees of freedom. Using A-(6) in A-(5) we have:

$$K = \begin{bmatrix} K_{ii} & K_{ij} & K_{ik} \\ & K_{jj} & K_{jk} \\ \text{symm.} & & K_{kk} \end{bmatrix} \qquad \text{A-(7)}$$

where $$K_{ii} = \left[C_i^T \bar{K}_i C_i + C_{ij}^T \bar{K}_{ij} C_{ij} + \bar{C}_{ki}^T \bar{K}_{ki} \bar{C}_{ki} \right] \qquad \text{A-(8)}$$

$$K_{ij} = \left[C_{ij}^T \bar{K}_{ij} \bar{C}_{ij} \right] \qquad \text{A-(9)}$$

$$K_{ik} = \left[\bar{C}_{ki}^T \bar{K}_{ki} C_{ki} \right] \qquad \text{A-(10)}$$

$$K_{jj} = \left[C_j^T \bar{K}_j C_j + \bar{C}_{ij}^T \bar{K}_{ij} \bar{C}_{ij} + C_{jk}^T \bar{K}_{jk} C_{jk} \right] \qquad \text{A-(11)}$$

$$K_{jk} = \left[C_{jk}^T K_{jk} \bar{C}_{jk} \right] \qquad \text{A-(12)}$$

$$K_{kk} = \left[C_k^T \bar{K}_k C_k + \bar{C}_{jk}^T \bar{K}_{jk} \bar{C}_{jk} + C_{ki}^T \bar{K}_{ki} C_{ki} \right] \qquad \text{A-(13)}$$

The 8×8 matrices give the stiffness coefficients of the Hrennikoff element. For example, the coefficients in the K_{ii} matrix are the stiffness coefficients giving the forces in the x_i direction at all eight grid points due to unit displacements of each of the eight grid points in the x_i direction. Using A-(7) the stiffness equation for the Hrennikoff element is:

$$\begin{bmatrix} K_{ii} & K_{ij} & K_{ik} \\ & K_{jj} & K_{jk} \\ \text{symm} & & K_{kk} \end{bmatrix} \begin{Bmatrix} r_i \\ r_j \\ r_k \end{Bmatrix} = \begin{Bmatrix} R_i \\ R_j \\ R_k \end{Bmatrix} \qquad \text{A-(14)}$$

Where, for example, r_i, and R_i are the displacement and force vector components in the x_i direction for the eight grid points of the Hrennikoff element. We will take the following definitions for the r_i, r_j, and r_k displacement vectors:

$$r_i = \begin{Bmatrix} r_{hi} \\ r_{ji} \\ r_{li} \\ r_{hi} \\ r_{gi} \\ r_{ii} \\ r_{ki} \\ r_{mi} \end{Bmatrix}, \quad r_j = \begin{Bmatrix} r_{ij} \\ r_{mj} \\ r_{jj} \\ r_{hj} \\ r_{gj} \\ r_{kj} \\ r_{hj} \\ r_{lj} \end{Bmatrix}, \quad r_k = \begin{Bmatrix} r_{kk} \\ r_{lk} \\ r_{mk} \\ r_{hk} \\ r_{gk} \\ r_{hk} \\ r_{ik} \\ r_{jk} \end{Bmatrix}$$

Where, for example, r_{hi} indicates the displacement at grid point h (see Figure 1) in the x_i direction. Using this definition and Equations A-(1) through A-(3) and A-(8) through A-(13) and also A-(15) the rod areas given by Equations (2) and (3) of Section 2, the stiffness matrices in Equation A-(14) are found to be as shown in Table 1.

The terms α_{ij}, α_{ki} are defined as:

$$\alpha_{ij} = \frac{\rho i}{\rho j}$$

also

$$V = a_i a_j a_k$$ = Volume contained by the Hrennikoff element.

Table 1

Hrennikoff Element Stiffness Matrix

$$K_{ii} = \frac{a_0^4 E}{10V} (\rho_j \rho_k)^2 \begin{bmatrix} 3 & 0 & 0 & 0 & -\beta_i & -\alpha_{ij}^2 & -\alpha_{ik}^2 & 0 \\ & 3 & 0 & 0 & -\alpha_{ij}^2 & -\beta_i & 0 & -\alpha_{ik}^2 \\ & & 3 & 0 & -\alpha_{ik}^2 & 0 & -\beta_i & -\alpha_{ij}^2 \\ & & & 3 & 0 & -\alpha_{ik}^2 & -\alpha_{ij}^2 & -\beta_i \\ & & & & 3 & 0 & 0 & 0 \\ & & & & & 3 & 0 & 0 \\ \text{Sym.} & & & & & & 3 & 0 \\ & & & & & & & 3 \end{bmatrix}$$

$$K_{ij} = \frac{a_0^4 E}{10V} (\rho_j \rho_k)^2 \begin{bmatrix} \alpha_{ij} & 0 & 0 & 0 & 0 & 0 & -\alpha_{ij} & 0 \\ 0 & 0 & \alpha_{ij} & 0 & -\alpha_{ij} & 0 & 0 & 0 \\ 0 & \alpha_{ij} & 0 & 0 & 0 & 0 & 0 & -\alpha_{ij} \\ 0 & 0 & 0 & \alpha_{ij} & 0 & -\alpha_{ij} & 0 & 0 \\ 0 & 0 & -\alpha_{ij} & 0 & \alpha_{ij} & 0 & 0 & 0 \\ -\alpha_{ij} & 0 & 0 & 0 & 0 & 0 & \alpha_{ij} & 0 \\ 0 & 0 & 0 & -\alpha_{ij} & 0 & \alpha_{ij} & 0 & 0 \\ 0 & -\alpha_{ij} & 0 & 0 & 0 & 0 & 0 & \alpha_{ij} \end{bmatrix}$$

Table 1 (Continued)

Hrennikoff Element Stiffness Matrix

$$K_{ik} = \frac{a_0^4 E}{10V} (\rho_j \rho_k)^2 \begin{bmatrix} \alpha_{ik} & 0 & 0 & 0 & 0 & -\alpha_{ik} & 0 & 0 \\ 0 & 0 & \alpha_{ik} & 0 & 0 & 0 & 0 & -\alpha_{ik} \\ 0 & \alpha_{ik} & 0 & 0 & -\alpha_{ik} & 0 & 0 & 0 \\ 0 & 0 & 0 & \alpha_{ik} & 0 & 0 & -\alpha_{ik} & 0 \\ 0 & -\alpha_{ik} & 0 & 0 & \alpha_{ik} & 0 & 0 & 0 \\ 0 & 0 & 0 & -\alpha_{ik} & 0 & 0 & \alpha_{ik} & 0 \\ -\alpha_{ik} & 0 & 0 & 0 & 0 & \alpha_{ik} & 0 & 0 \\ 0 & 0 & -\alpha_{ik} & 0 & 0 & 0 & 0 & \alpha_{ik} \end{bmatrix}$$

$$K_{jj} = \frac{a_0^4 E}{10V} (\rho_k \rho_i)^2 \begin{bmatrix} 3 & 0 & 0 & 0 & -\beta_j & -\alpha_{jk}^2 & -\alpha_{ji}^2 & 0 \\ & 3 & 0 & 0 & -\alpha_{jk}^2 & -\beta_j & 0 & -\alpha_{ji}^2 \\ & & 3 & 0 & -\alpha_{ji}^2 & 0 & -\beta_j & -\alpha_{jk}^2 \\ & & & 3 & 0 & -\alpha_{ji}^2 & -\alpha_{jk}^2 & -\beta_j \\ & & & & 3 & 0 & 0 & 0 \\ \text{Sym.} & & & & & 3 & 0 & 0 \\ & & & & & & 3 & 0 \\ & & & & & & & 3 \end{bmatrix}$$

Table 1 (Continued)

Hrennikoff Element Stiffness Matrix

$$K_{jk} = \frac{a_0^4 E}{10V} (\rho_k \rho_i)^2 \begin{bmatrix} \alpha_{jk} & 0 & 0 & 0 & 0 & 0 & -\alpha_{jk} & 0 \\ 0 & 0 & \alpha_{jk} & 0 & -\alpha_{jk} & 0 & 0 & 0 \\ 0 & \alpha_{jk} & 0 & 0 & 0 & 0 & 0 & -\alpha_{jk} \\ 0 & 0 & 0 & \alpha_{jk} & 0 & -\alpha_{jk} & 0 & 0 \\ 0 & 0 & -\alpha_{jk} & 0 & \alpha_{jk} & 0 & 0 & 0 \\ -\alpha_{jk} & 0 & 0 & 0 & 0 & 0 & \alpha_{jk} & 0 \\ 0 & 0 & 0 & -\alpha_{jk} & 0 & \alpha_{jk} & 0 & 0 \\ 0 & -\alpha_{jk} & 0 & 0 & 0 & 0 & 0 & \alpha_{jk} \end{bmatrix}$$

$$K_{kk} = \frac{a_0^4 E}{10V} (\rho_i \rho_j)^2 \begin{bmatrix} 3 & 0 & 0 & 0 & -\beta_k & -\alpha_{ki}^2 & -\alpha_{kj}^2 & 0 \\ & 3 & 0 & 0 & -\alpha_{ki}^2 & -\beta_k & 0 & -\alpha_{kj}^2 \\ & & 3 & 0 & -\alpha_{kj}^2 & 0 & -\beta_k & -\alpha_{ki}^2 \\ & & & 3 & 0 & -\alpha_{kj}^2 & -\alpha_{ki}^2 & -\beta_k \\ & & & & 3 & 0 & 0 & 0 \\ & & & & & 3 & 0 & 0 \\ \text{Sym.} & & & & & & 3 & 0 \\ & & & & & & & 3 \end{bmatrix}$$